

# Comparative study of the phonons in nonsuperconducting BaC<sub>6</sub> and superconducting CaC<sub>6</sub> using inelastic x-ray scattering

A. C. Walters,<sup>1,2,\*</sup> C. A. Howard,<sup>2</sup> M. H. Upton,<sup>3,4</sup> M. P. M. Dean,<sup>4</sup> A. Alatas,<sup>3</sup> B. M. Leu,<sup>3</sup> M. Ellerby,<sup>2</sup> D. F. McMorrow,<sup>2</sup> J. P. Hill,<sup>4</sup> M. Calandra,<sup>5</sup> and F. Mauri<sup>5</sup>

<sup>1</sup>ESRF, Polygone Scientifique Louis Néel, 6 rue Jules Horowitz, F-38000 Grenoble, France

<sup>2</sup>London Centre for Nanotechnology and Department of Physics and Astronomy, University College London, London WC1E 6BT, United Kingdom

<sup>3</sup>Advanced Photon Source, Argonne National Laboratory, Argonne, Illinois 60439, USA

<sup>4</sup>Condensed Matter Physics and Materials Science Department, Brookhaven National Laboratory, Upton, New York 11973, USA

<sup>5</sup>Université Pierre et Marie Curie, 4 Place Jussieu-case postale 115, F-72252 Paris Cedex 05, France

(Received 3 February 2011; revised manuscript received 31 March 2011; published 25 July 2011)

The low-energy phonons of two different graphite intercalation compounds (GICs) have been measured as a function of temperature using inelastic x-ray scattering (IXS). In the case of the non-superconductor BaC<sub>6</sub>, the phonons observed are significantly higher (up to 20%) in energy than those predicted by theory, in contrast to the reasonable agreement found in superconducting CaC<sub>6</sub>. Additional IXS intensity is observed below 15 meV in both BaC<sub>6</sub> and CaC<sub>6</sub>. It has been previously suggested that this additional inelastic intensity may arise from defect or vacancy modes not predicted by theory [d'Astuto *et al.*, *Phys. Rev. B* **81**, 104519 (2010)]. Here it is shown that this additional intensity can arise directly from the polycrystalline nature of the available samples. Our results show that future theoretical work is required to understand the relationship between the crystal structure, the phonons, and the superconductivity in GICs.

DOI: [10.1103/PhysRevB.84.014511](https://doi.org/10.1103/PhysRevB.84.014511)

PACS number(s): 74.25.Kc, 71.20.Tx, 63.20.K-, 78.70.Ck

## I. INTRODUCTION

Since the discovery of superconductivity in YbC<sub>6</sub> ( $T_c = 6.5$  K) and CaC<sub>6</sub> ( $T_c = 11.5$  K) at temperatures over an order of magnitude higher than previously found in graphite intercalation compounds (GIC's),<sup>1,2</sup> the properties of this family of GICs have been studied extensively using a variety of different experimental techniques.<sup>3-8</sup> Although initially an exotic superconducting mechanism was proposed involving acoustic plasmons,<sup>9</sup> subsequent density functional theory (DFT) studies described the superconductivity via a more orthodox electron-phonon ( $e$ -ph) coupling mechanism with  $s$ -wave symmetry.<sup>10-13</sup> These DFT descriptions predicted that the  $e$ -ph coupling is approximately equal for phonons associated with vibration of the carbon atoms and for phonons associated with movement of the intercalant calcium.

At present, there are experimental studies in the literature that give conflicting viewpoints concerning the nature of the  $e$ -ph coupling in GICs. A large Ca isotope effect [ $\alpha(\text{Ca}) \sim 0.5$ ] has been measured in CaC<sub>6</sub>,<sup>6</sup> which, if viewed within the BCS description of superconductivity, suggests that only the phonons due to the vibration of calcium are involved in the electron pairing. In contrast, angle-resolved photoemission spectroscopy (ARPES) measurements on CaC<sub>6</sub> (Ref. 8) have found that the  $e$ -ph coupling to graphite-like high-energy phonons is so strong that it can explain the superconducting transition temperature alone, without any additional coupling to calcium phonons. These discrepancies point to the need for a detailed study of the phonons in GICs, both to test the DFT description and to look for direct evidence for  $e$ -ph coupling involving specific phonons. Moreover, phonon studies in graphitic systems in general are important as the electron-phonon interactions in these systems are under much scrutiny.<sup>14-16</sup>

Superconductivity in GICs is directly linked to the graphite layer separation, with the superconducting transition temperature  $T_c$  increasing as the graphite layer separation  $d$  is reduced. This trend is supported both by the observed values of  $T_c$  in a variety of GICs (Ref. 5) and by measurements of  $T_c$  as a function of pressure in CaC<sub>6</sub> (Ref. 17) and YbC<sub>6</sub>.<sup>18</sup> Indeed, in BaC<sub>6</sub> the graphite layer separation is so large that superconductivity appears to be suppressed entirely, with no superconducting transition observed down to 0.080 K.<sup>19</sup> It is therefore instructive to study the superconductivity in GICs by studying GICs with different intercalants, since by changing the intercalant one changes  $d$  and therefore tunes  $T_c$ .

In this paper, we present the low-energy phonon dispersions in nonsuperconducting BaC<sub>6</sub> and superconducting CaC<sub>6</sub> as measured using inelastic x-ray scattering (IXS). These data represent the first momentum-resolved phonon measurements on BaC<sub>6</sub>. We find a substantial discrepancy between experiment and theory in the phonon energies of BaC<sub>6</sub>, in contrast to the good agreement in the case of CaC<sub>6</sub>. Like many other layered materials, GIC's are difficult to synthesize as high-quality single crystals. We demonstrate here that the details of the preferred orientation (texture) of the crystallites in these GIC samples can lead to the observation of phonons that, because of their polarization, are theoretically forbidden to be observed. Our work highlights the importance of accounting for these effects in phonon studies of textured polycrystalline samples and calls for the need for single-crystal GIC samples to address the role of the electron-phonon coupling in these materials.

The low-energy phonons in CaC<sub>6</sub> have been measured previously<sup>20</sup> and found to be in good overall agreement with the published DFT calculations. Subsequent to this work, two momentum-resolved phonon studies have been performed

on  $\text{CaC}_6$ : an inelastic neutron scattering (INS) study, which concentrates primarily on the high-energy graphitelike phonon modes,<sup>21</sup> and a study of the low-energy phonons in  $\text{CaC}_6$  performed using both IXS and INS.<sup>22</sup> While in Ref. 21 good agreement was found with the calculated DFT phonon dispersions by taking into account the polycrystalline nature of the sample, in Ref. 22 it was suggested that an additional phonon mode exists in  $\text{CaC}_6$  of uncertain origin. Here we propose an alternative explanation: the additional IXS intensity arises from the weak crystallographic texture in the polycrystalline GIC samples.

## II. EXPERIMENTAL METHODS

The GIC samples were made using ZYA grade highly orientated pyrolytic graphite (HOPG) platelets purchased from GE Advanced Ceramics. The  $\text{BaC}_6$  sample was made using the vapor transport method.<sup>23</sup> An HOPG platelet was outgassed at 500 °C and then sealed into a quartz tube along with the barium metal (purity >99.99%) under high vacuum ( $<10^{-6}$  mbar). The tube was then heated to 490 °C and maintained at this temperature for 4 weeks. The  $\text{CaC}_6$  samples used were prepared by immersing a HOPG platelet in a Li-Ca alloy for 10 days, as described elsewhere.<sup>24</sup>  $\text{CaC}_6$  samples taken from the same batch were found to have a sharp superconducting transition at 11.5 K from magnetic susceptibility measurements. The very high purity of the samples (>99% pure in both cases) can be seen in the  $(00l)$  diffraction shown in Figs. 1(e) and 1(f), where there are no visible Bragg peaks from any impurities.

The starting graphite (HOPG) is composed of small crystallites ( $\approx 1 \mu\text{m}$ ), which have a strong preferred orientation (strong texture) perpendicular to the graphene planes (out-of-plane), giving a  $(00l)$  mosaic with a full width at half-maximum (FWHM) as low as  $0.2^\circ$ . However, within the graphene planes (in-plane), the crystallites are orientated randomly.<sup>23</sup> After intercalation, the crystallites are still orientated randomly in-plane, but out-of-plane the orientation of the crystallites is more random, with the GIC's studied here having  $(00l)$  mosaics of  $5^\circ$ . This means that the texture is weaker in the GIC samples than in HOPG, since a weaker texture means that the samples are more like perfect powders, which have zero texture.

$\text{CaC}_6$  has the structure  $R\bar{3}m$ , which can be described using a rhombohedral or a hexagonal basis.<sup>2</sup> The calcium atoms are arranged in three different ways in different intercalant layers (called  $A\alpha A\beta A\gamma$  stacking, where the Roman letters define graphite layers and the Greek letters define intercalant layers). The crystal structure of  $\text{CaC}_6$  in the hexagonal basis is shown in Fig. 1(b), and the shape of the first Brillouin zone is shown in Fig. 1(d). Here we define the reciprocal-lattice directions using the hexagonal basis, meaning that the out-of-plane direction is the  $(00l)$  direction. This convention aids comparison with the  $\text{BaC}_6$  data, as  $\text{BaC}_6$  has the space group  $P6_3/mmc$ , which is normally described within the hexagonal basis. The stacking in  $\text{BaC}_6$  is  $A\alpha A\beta$ , as shown in Fig. 1(a). The first Brillouin zone of  $\text{BaC}_6$  is presented in Fig. 1(c). The lattice parameters of  $\text{CaC}_6$  are  $a = 4.333(2) \text{ \AA}$  and  $c = 13.572(2) \text{ \AA}$ ,<sup>25</sup> giving a graphite layer separation  $d$  of  $4.524(1) \text{ \AA}$ , and in  $\text{BaC}_6$  the

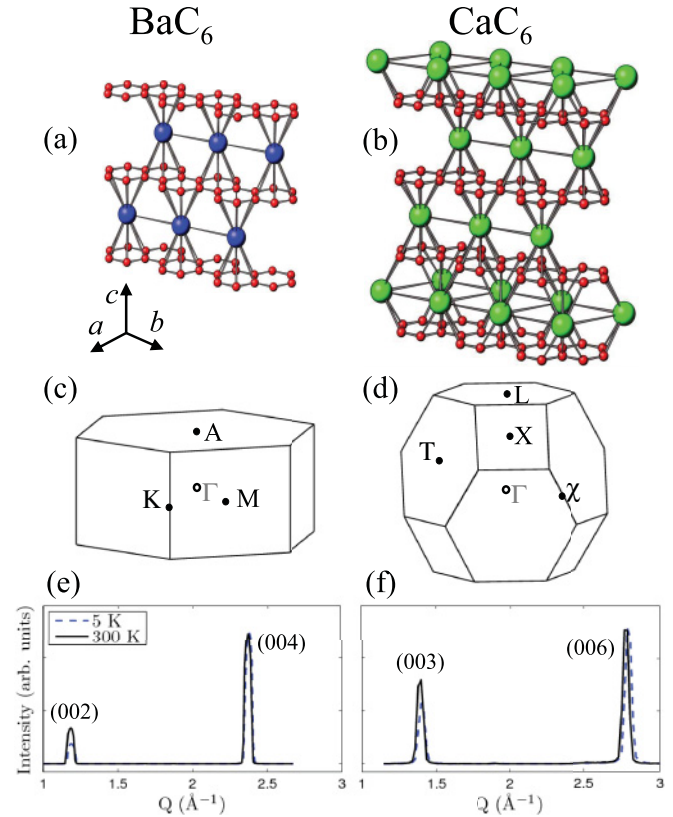


FIG. 1. (Color online) The structural properties of  $\text{BaC}_6$  and  $\text{CaC}_6$ : (a) and (b) Crystal structure, (c) and (d) first Brillouin zone with symmetry points, (e) and (f) diffraction on  $\text{BaC}_6$  and  $\text{CaC}_6$  measured in the  $(00l)$  direction at 5 K (dashed blue line) and 300 K (solid black line) at 3-ID. The symmetry points shown are at the edge of the Brillouin zone apart from the  $\Gamma$  point, which is at the zone center. There is practically no signal from impurities in the  $(00l)$  diffraction from either sample.

lattice parameters are  $a = 4.302(6) \text{ \AA}$  and  $c = 10.50(4) \text{ \AA}$  with  $d = 5.25(2) \text{ \AA}$ .<sup>26</sup>

The IXS measurements were performed at 3-ID at the Advanced Photon Source, Argonne National Laboratory, with an incident x-ray energy of 21.657 keV,<sup>27</sup> providing an energy resolution between 2.2 and 2.4 meV, depending on the specific analyzer. The spectrometer has four analyzers, allowing energy scans to be done at different momentum transfers simultaneously. The momentum resolution in all cases was  $0.072 \text{ \AA}^{-1}$  in the scattering plane and  $0.183 \text{ \AA}^{-1}$  perpendicular to it. The phonon peaks were fitted with pseudo-Voigt functions, which were appropriately scaled by the Bose factor. The phonon dispersions were produced by plotting the peak positions as a function of the phonon wave vector  $\mathbf{q}$ , defined within the equation  $\mathbf{Q} = \mathbf{G} + \mathbf{q}$ , where  $\mathbf{G}$  is the nearest reciprocal-lattice vector and  $\mathbf{Q}$  is the momentum transfer.

To model the effect of the crystallographic texture in the GIC samples on the phonon spectra, simulations of the IXS data were produced by summing hundreds of simulated IXS intensities, each of which was performed at a specific momentum transfer. The crystallographic texture was described by performing simulations over a volume in

reciprocal space expressed in spherical polar coordinates ( $|\mathbf{Q}|, \theta, \phi$ ), where  $\theta$  has its rotation axis out-of-plane. For the two-dimensional (2D) powder simulations, the momentum transfers were selected using Lorentzian sampling of  $\phi$  with a FWHM of  $5^\circ$  and allowing  $\theta$  to take any value. For the 3D powder simulations, both  $\phi$  and  $\theta$  were allowed to take any value. The summed IXS spectra were then convolved with the momentum and energy resolution of the IXS spectrometer. This method was also used in our recent INS study of  $\text{CaC}_6$ .<sup>21</sup>

The two-dimensionality of these GIC's, together with the significant difference in mass between the intercalant and carbon, means that the phonon modes can be separated, to a good approximation, into four groups:  $I_{xy}$ ,  $I_z$ ,  $C_{xy}$ , and  $C_z$ , where  $I_{xy}$  describes phonon modes purely due to vibrations of intercalant atoms in-plane,  $I_z$  denotes the intercalant phonons out-of-plane, and  $C_{xy(z)}$  denotes the equivalent carbon in-plane (out-of-plane) phonons.

### III. INELASTIC X-RAY SCATTERING MEASUREMENTS

#### A. Phonons in $\text{BaC}_6$

The (00 $l$ ) phonon dispersions of  $\text{BaC}_6$  measured at both 5 and 300 K are plotted in Fig. 2, together with calculated dispersions.<sup>11</sup> The measured  $\text{Ba}_z$  phonon branches are significantly higher in energy than the theoretical values: near the edge of the Brillouin zone, at symmetry point A, the measured phonon energy for the optic  $\text{Ba}_z$  mode is almost 20% larger than that predicted. In addition, in all of the measured IXS energy scans on  $\text{BaC}_6$ , there is additional intensity observed below 10 meV, plotted with full symbols, which is not predicted by theory.

So what is the origin of this discrepancy between experiment and theory in  $\text{BaC}_6$ ? We consider a number of possibilities. The DFT calculations were performed using a different structure from the structure experimentally determined, which may have affected their results. In addition, the charge transfer from the Ba atoms to the graphene planes may be inaccurately predicted by theory. Finally, the calculations do not account for the polycrystallinity of the real samples, so part of the disagreement may be due to their crystallographic texture.

The published calculations for  $\text{BaC}_6$  use lattice parameters equivalent to  $a = 4.350 \text{ \AA}$  and  $c = 10.40 \text{ \AA}$ ,<sup>11</sup> which are significantly different from the values found via x-ray diffraction [ $a = 4.302(6) \text{ \AA}$  and  $c = 10.50(4) \text{ \AA}$ ].<sup>26</sup> In addition, the space group of  $\text{CaC}_6$  ( $R = 3m$ ) is used for  $\text{BaC}_6$  in the calculation, rather than the experimentally found  $P6_3/mmc$ . To determine whether the observed discrepancy arises because of these structural differences, we performed an additional phonon calculation at the  $\Gamma$  point using the experimental structure and lattice parameters, as shown in Fig. 2 (crosses). This calculation gives phonon energies in approximate agreement with the previous calculation, showing that the calculations are largely insensitive to small changes in both the lattice parameters and the space group. Therefore, the incorrect structure used in the initial calculations can be eliminated as a cause of the discrepancies.

Another possibility is that the charge transfer from the Ba atoms to the graphite has been underestimated theoretically. If there is less charge than predicted in the graphitic  $\pi^*$  bands,

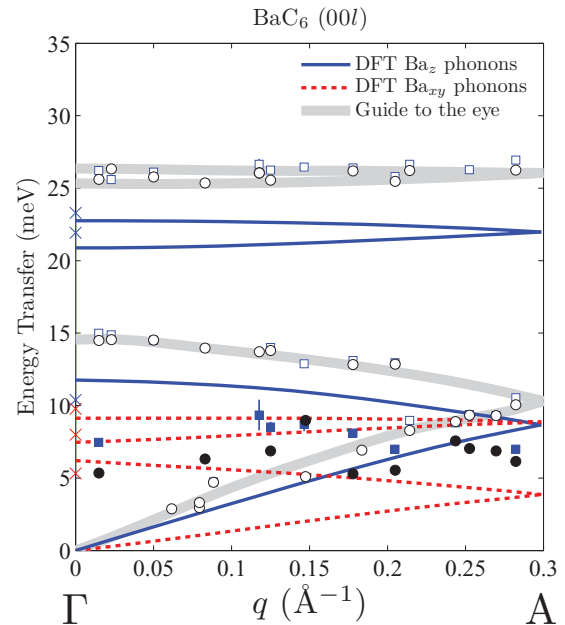


FIG. 2. (Color online)  $\text{BaC}_6$  (00 $l$ ) phonon dispersion measured at 5 K (squares) and 300 K (circles). Empty symbols denote  $\text{Ba}_z$  phonon intensity, full symbols label  $\text{Ba}_{xy}$  phonon intensity. The  $\text{Ba}_{xy}$  phonons should not be visible in this scattering geometry (see text). The theoretical dispersion of the  $\text{Ba}_z$  and  $\text{Ba}_{xy}$  phonons is plotted with solid lines and dashed lines, respectively.<sup>11</sup> A guide to the eye is plotted showing the dispersion of the  $\text{Ba}_z$  phonons at 300 K (thick solid line). The symmetry point A is located at  $q = 0.299 \text{ \AA}^{-1}$ . The crosses mark the phonon energies calculated at  $\Gamma$  using the experimental lattice parameters and space group of  $\text{BaC}_6$ .

then the bonds should be stronger than predicted, since filling the antibonding  $\pi^*$  band destabilizes the bonds. Stronger bonds lead directly to higher phonon energies. The effect of charge transfer on phonons in GIC's has been predicted theoretically<sup>28</sup> and observed using Raman scattering.<sup>16</sup> This would explain why the phonons are higher in energy than predicted, but it cannot explain why additional intensity is observed below 10 meV.

The additional phonon intensity can be explained as a result of the crystallographic texture of the GIC samples. Here we argue that this signal arises from the excitation of  $I_{xy}$  phonons over a large volume in reciprocal space due to the weak crystallographic texture. For an ideal single crystal, and perfect instrumental resolution, the  $I_{xy}$  phonons are disallowed (their intensity is zero) when  $\mathbf{Q}$  is completely out-of-plane due to the  $\mathbf{Q} \cdot \mathbf{e}(\mathbf{q})$  term in the IXS phonon cross section, where  $\mathbf{e}(\mathbf{q})$  is the eigenvector of the phonon with wave vector  $\mathbf{q}$ .<sup>29</sup> However, in the case of the polycrystalline GIC samples studied, the weak crystallographic texture provides an explanation for the observation of the  $I_{xy}$  phonons. Even if the nominal momentum  $\mathbf{Q}$  is entirely out-of-plane, the large reciprocal space volume integrated over in each measurement due to the weak preferred orientation of the crystallites will include many values of  $\mathbf{Q}$  that have a significant component in-plane. This effect is discussed further in Sec. IV.

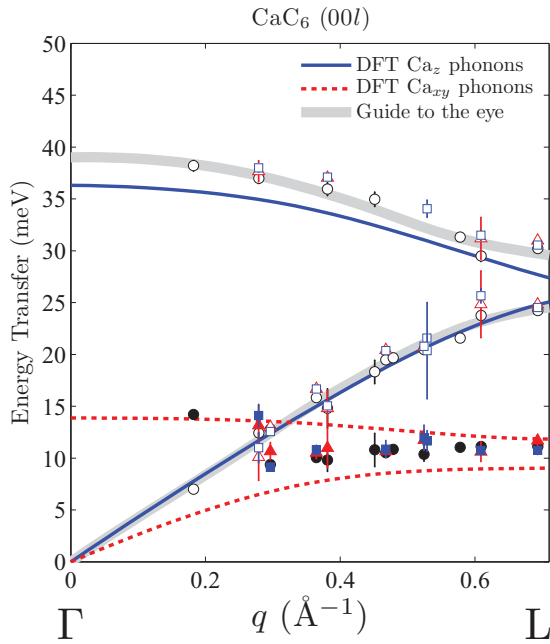


FIG. 3. (Color online)  $\text{CaC}_6$  (00 $l$ ) phonon dispersion measured at 5 K (squares), 50 K (triangles), and 300 K (circles). Empty symbols denote  $\text{Ca}_z$  phonon intensity, full symbols label  $\text{Ca}_{xy}$  phonon intensity. The  $\text{Ca}_{xy}$  phonons should not be visible in this scattering geometry (see text). The theoretical dispersion of the  $\text{Ca}_z$  and  $\text{Ca}_{xy}$  phonons is plotted with solid lines and dashed lines, respectively.<sup>10</sup> A guide to the eye is plotted showing the dispersion of the experimental  $\text{Ca}_z$  phonons at 300 K (thick solid line). The symmetry point  $L$  is located at  $q = 0.694 \text{ \AA}^{-1}$ .

### B. Phonons in $\text{CaC}_6$

Figure 3 presents the (00 $l$ ) phonon dispersion in  $\text{CaC}_6$  at 5, 50, and 300 K. A subset of the  $\text{CaC}_6$  data has already been published,<sup>20</sup> but the scope of the data presented here is much more extensive. The additional phonon intensity below 15 meV again results from the large mosaic of the sample and is discussed at length in Sec. IV. The phonon dispersions calculated using DFT are plotted in the same figure.<sup>10</sup> The two  $\text{Ca}_z$  modes are well described by the DFT calculations over the whole  $Q$  range sampled, especially in the case of the acoustic  $\text{Ca}_z$  mode. The higher-energy mode, which disperses between 30 and 40 meV (the optic  $\text{Ca}_z$  mode), is about 2 meV higher in energy than predicted, but the character of the dispersion is reasonably well described.

In both  $\text{CaC}_6$  and  $\text{BaC}_6$ , the energies of the  $I_z$  modes are slightly hardened ( $<1$  meV) upon cooling from 300 to 5 K, but there is no observable difference in  $\text{CaC}_6$  between the data measured above and below  $T_c$ . The small temperature dependence most likely results from the reduction in the  $c$  lattice parameter upon cooling, visible in the diffraction presented in Figs. 1(e) and 1(f).

## IV. MODELING THE CRYSTALLOGRAPHIC TEXTURE IN $\text{BaC}_6$ AND $\text{CaC}_6$

In Figs. 4 and 5, a selection of phonon spectra measured at 300 K in the (00 $l$ ) direction in  $\text{BaC}_6$  and  $\text{CaC}_6$  is presented. In both cases, two phonons are observed in the raw IXS data

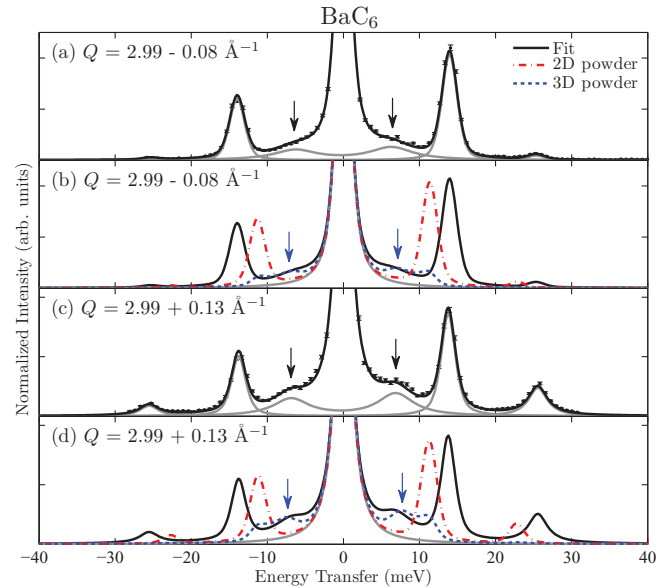


FIG. 4. (Color online) (a) (00 $l$ ) IXS data at  $Q = 2.91 \text{ \AA}^{-1}$  on  $\text{BaC}_6$  at 300 K, plotted with the data fit and the decomposed fitted phonon peaks. (b) Fit to the data at  $Q = 2.91 \text{ \AA}^{-1}$ , plotted with the fitted elastic line and against IXS simulations based on *ab initio* calculations<sup>11</sup> that use the 2D powder model and the 3D powder model described in the text. (c) and (d) Same as (a) and (b) but for  $Q = 3.12 \text{ \AA}^{-1}$ . In each panel, the experimental (simulated) IXS intensity due to  $\text{Ba}_{xy}$  phonons is marked with black (blue) arrows.

(the acoustic and optic  $I_z$  branches), as well as additional IXS intensity at low energies. In each of the panels, two IXS simulations are plotted. The first simulation models the sample as a 2D powder: that is, the crystallites have no preferred orientation in-plane, but they have a Lorentzian mosaic of  $\text{FWHM} = 5^\circ$  out-of-plane, consistent with our x-ray diffraction. The second simulation models the sample with no preferred orientation (no texture), i.e., as a 3D powder. Both simulations are added to the experimental elastic intensity.

In the case of  $\text{BaC}_6$ , plotted in Fig. 4, the overall agreement is better with the 2D powder model than with the 3D powder model, especially in the ratio between the acoustic and optic  $\text{Ba}_z$  phonons. However, in the 2D powder model, the IXS intensity due to the  $\text{Ba}_{xy}$  phonons is much smaller than measured. The additional features predicted by the 3D powder model are similar to those observed, but there the intensities of the  $\text{Ba}_z$  phonons are underestimated. These observations suggest that perhaps the crystallographic texture of the  $\text{BaC}_6$  samples is weaker than expected from our x-ray diffraction, lying somewhere between the 2D and 3D powder models.

In the  $\text{CaC}_6$  data in Fig. 5, the low-energy IXS features look qualitatively similar to the  $\text{Ca}_{xy}$  features predicted by the 3D powder model. However, the 3D powder description of  $\text{CaC}_6$  is once again not a satisfactory description, as the intensity of the  $\text{Ca}_z$  phonons is underestimated in most cases and the IXS intensity at low energies is significantly overestimated.<sup>30</sup> The measured  $\text{CaC}_6$  data appear to lie somewhere between the 2D and 3D powder simulations, similar to the  $\text{BaC}_6$  data, although the  $\text{CaC}_6$  appears to be more like the 3D powder than  $\text{BaC}_6$ .

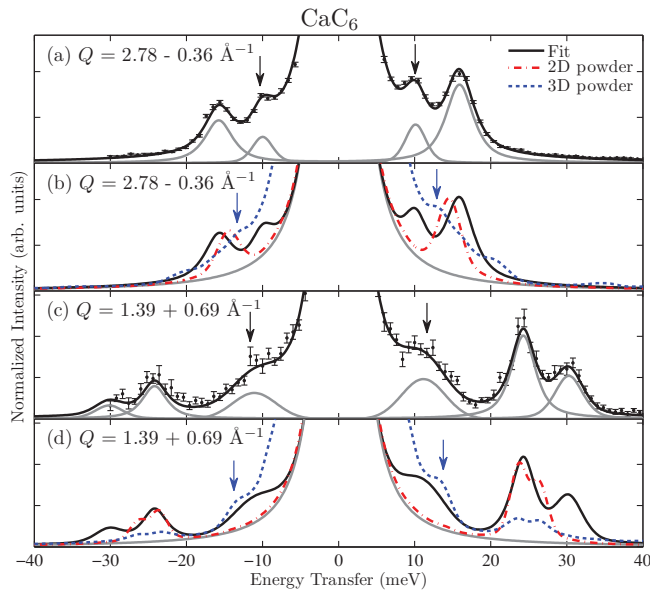


FIG. 5. (Color online) (a)  $(00l)$  IXS data at  $Q = 2.42 \text{ \AA}^{-1}$  on  $\text{CaC}_6$  at 300 K, plotted with the data fit and the decomposed fitted phonon peaks. (b) Fit to the data at  $Q = 2.42 \text{ \AA}^{-1}$ , plotted with the fitted elastic line and against IXS simulations based on *ab initio* calculations<sup>10</sup> that use the 2D powder model and the 3D powder model described in the text. (c) and (d) Same as (a) and (b) but for  $Q = 2.08 \text{ \AA}^{-1}$ . In each panel, the experimental (simulated) IXS intensity due to  $\text{Ca}_{xy}$  phonons is marked with black (blue) arrows.

This suggests that the distribution of intercalant atoms in  $\text{CaC}_6$  is rather random, which is consistent with the behavior of  $\text{CaC}_6$  under pressure as studied with x-ray diffraction, where the Ca atoms are found to be very mobile.<sup>4</sup> More theoretical and experimental work is required to understand the complicated crystallographic texture of GIC's, with more extensive x-ray diffraction being a natural starting point.

A recent IXS and INS study by d'Astuto *et al.*<sup>22</sup> on  $\text{CaC}_6$  suggested that the additional inelastic intensity was due to an interaction with the acoustic  $\text{Ca}_z$  mode, causing an avoided crossing, or anticrossing, which is seen as a splitting in the acoustic  $\text{Ca}_z$  mode. Their work was supplemented by INS data, which allowed them to more easily access momenta nearer to the  $\Gamma$  point. The study concluded that the additional inelastic intensity could be due to a defect or vacancy mode. Although we cannot exclude this hypothesis, our simulations suggest that if the orientation of the crystallites in these samples is more random than previously thought, the weak crystallographic texture can account for the anomalous features without recourse to such a mode.

## V. CONCLUSIONS

To summarize, the dispersions of the low-energy phonons in  $\text{BaC}_6$  and  $\text{CaC}_6$  have been measured as a function of temperature using inelastic x-ray scattering. In  $\text{BaC}_6$  the experimental and DFT-calculated phonon dispersions<sup>11</sup> disagree, with measured phonon energies up to 20% higher than predicted. We suggest that this large discrepancy may result from an underestimation of the charge transfer from the Ba atoms to the graphite sheets in the theory. Our work motivates further study on  $\text{BaC}_6$  to examine the underlying reasons for this disagreement. In contrast, reasonable agreement with theory is found in  $\text{CaC}_6$  for the  $\text{Ca}_z$  phonons. This consistency between theory and experiment provides indirect supporting evidence for the DFT description<sup>10</sup> of the superconductivity in  $\text{CaC}_6$ .

No signatures of electron-phonon coupling are observed in the phonon dispersions or the phonon widths in either non-superconducting  $\text{BaC}_6$  or superconducting  $\text{CaC}_6$ , despite the drastically different superconducting transitions of these related compounds. In both  $\text{BaC}_6$  and  $\text{CaC}_6$  there is a small ( $<1$  meV) hardening of the  $I_z$  phonons as the temperature is decreased, but this is likely due to a reduction in the  $c$  lattice parameter and is unaffected by the presence of superconductivity in  $\text{CaC}_6$  below 11.5 K. The largest source of phonon broadening experimentally is very likely the weak crystallographic texture inherent in the GIC samples.

Finally, the IXS simulations presented here show that weak crystallographic texture in polycrystalline GIC samples may lead to additional inelastic intensity from  $I_{xy}$  phonons. Such additional intensity has been observed recently in  $\text{CaC}_6$  (Refs. 20 and 22) and  $\text{YbC}_6$ ,<sup>31</sup> but also in older INS studies on  $\text{RbC}_{24}$  (Ref. 32) and  $\text{KC}_{24}$ .<sup>33</sup> This work provides a timely reminder that the crystallographic texture inherent in many graphitic systems may give rise to unexpected experimental effects.

## ACKNOWLEDGMENTS

We would like to thank Matteo d'Astuto and Michael Krisch for illuminating discussions. A.C.W. would like to thank Ian Wood and Richard Thanki for their assistance and the EPSRC and STFC for funding. Calculations were performed at the IDRIS supercomputing center (project 081202). The work at Brookhaven is supported in part by the US DOE under Contract No. DE-AC02-98CH10886 and in part by the Center for Emergent Superconductivity, an Energy Frontier Research Center funded by the US DOE, Office of Basic Energy Sciences. The work at the Advanced Photon Source was supported by the US DOE, Office of Basic Energy Sciences, under Contract No. DE-AC02-06CH11357.

\*andrew.walters@esrf.fr

<sup>1</sup>T. E. Weller, M. Ellerby, S. S. Saxena, R. P. Smith, and N. T. Skipper, *Nat. Phys.* **1**, 39 (2005).

<sup>2</sup>N. Emery, C. Hérold, M. d'Astuto, V. Garcia, Ch. Bellin, J. F. Marêché, P. Lagrange, and G. Loupiau, *Phys. Rev. Lett.* **95**, 087003 (2005).

<sup>3</sup>R. Cubitt, J. S. White, M. Laver, M. R. Eskildsen, C. D. Dewhurst, D. M. Paul, A. J. Crichton, M. Ellerby, C. Howard, Z. Kurban, and F. Norris, *Phys. Rev. B* **75**, 140516(R) (2007).

<sup>4</sup>A. Gauzzi, N. Bendiab, M. d'Astuto, B. Canny, M. Calandra, F. Mauri, G. Loupiau, N. Emery, C. Hérold, P. Lagrange, M. Hanfland, and M. Mezouar, *Phys. Rev. B* **78**, 064506 (2008).

- <sup>5</sup>J. S. Kim, L. Boeri, J. R. O'Brien, F. S. Razavi, and R. K. Kremer, *Phys. Rev. Lett.* **99**, 027001 (2007).
- <sup>6</sup>D. G. Hinks, D. Rosenmann, H. Claus, M. S. Bailey, and J. D. Jorgensen, *Phys. Rev. B* **75**, 014509 (2007).
- <sup>7</sup>R. S. Gonnelli, D. Daghero, D. Delaude, M. Tortello, G. A. Ummarino, V. A. Stepanov, J. S. Kim, R. K. Kremer, A. Sanna, G. Profeta, and S. Massidda, *Phys. Rev. Lett.* **100**, 207004 (2008).
- <sup>8</sup>T. Valla, J. Camacho, Z.-H. Pan, A. V. Fedorov, A. C. Walters, C. A. Howard, and M. Ellerby, *Phys. Rev. Lett.* **102**, 107007 (2009).
- <sup>9</sup>G. Csányi, P. B. Littlewood, A. H. Nevidomskyy, C. J. Pickard, and B. D. Simons, *Nat. Phys.* **1**, 42 (2005).
- <sup>10</sup>M. Calandra and F. Mauri, *Phys. Rev. Lett.* **95**, 237002 (2005).
- <sup>11</sup>M. Calandra and F. Mauri, *Phys. Rev. B* **74**, 094507 (2006).
- <sup>12</sup>A. Sanna, G. Profeta, A. Floris, A. Marini, E. K. U. Gross, and S. Massidda, *Phys. Rev. B* **75**, 020511 (2007).
- <sup>13</sup>M. Calandra, G. Profeta, and F. Mauri, *Phys. Rev. B* **82**, 165111 (2010).
- <sup>14</sup>S. Pisana, M. Lazzeri, C. Casiraghi, K. S. Novoselov, A. K. Geim, A. C. Ferrari, and F. Mauri, *Nat. Mater.* **6**, 198 (2007).
- <sup>15</sup>M. Lazzeri and F. Mauri, *Phys. Rev. Lett.* **97**, 266407 (2006).
- <sup>16</sup>M. P. M. Dean, C. A. Howard, S. S. Saxena, and M. Ellerby, *Phys. Rev. B* **81**, 045405 (2010).
- <sup>17</sup>A. Gauzzi, S. Takashima, N. Takeshita, C. Terakura, H. Takagi, N. Emery, C. Hérold, P. Lagrange, and G. Loupías, *Phys. Rev. Lett.* **98**, 067002 (2007).
- <sup>18</sup>R. P. Smith, A. Kusmartseva, Y. T. C. Ko, S. S. Saxena, A. Akrap, L. Forro, M. Laad, T. E. Weller, M. Ellerby, and N. T. Skipper, *Phys. Rev. B* **74**, 024505 (2006).
- <sup>19</sup>S. Nakamae, A. Gauzzi, F. Ladieu, D. L'Hôte, N. Eméry, C. Hérold, J. F. Marêché, P. Lagrange, and G. Loupías, *Solid State Commun.* **145**, 493 (2008).
- <sup>20</sup>M. H. Upton, A. C. Walters, C. A. Howard, K. C. Rahnejat, M. Ellerby, J. P. Hill, D. F. McMorrow, A. Alatas, B. M. Leu, and W. Ku, *Phys. Rev. B* **76**, 220501(R) (2007).
- <sup>21</sup>M. P. M. Dean, A. C. Walters, C. A. Howard, T. E. Weller, M. Calandra, F. Mauri, M. Ellerby, S. S. Saxena, A. Ivanov, and D. F. McMorrow, *Phys. Rev. B* **82**, 014533 (2010).
- <sup>22</sup>M. d'Astuto, M. Calandra, N. Bendiab, G. Loupías, F. Mauri, S. Zhou, J. Graf, A. Lanzara, N. Emery, C. Hérold, P. Lagrange, D. Petitgrand, and M. Hoesch, *Phys. Rev. B* **81**, 104519 (2010).
- <sup>23</sup>M. S. Dresselhaus and G. Dresselhaus, *Adv. Phys.* **51**, 1 (2002).
- <sup>24</sup>S. Pruvost, C. Hérold, A. Hérold, and P. Lagrange, *Carbon* **42**, 1825 (2004).
- <sup>25</sup>N. Emery, C. Hérold, and P. Lagrange, *J. Solid State Chem.* **178**, 2947 (2005).
- <sup>26</sup>D. Guerard, M. C haabouni, P. Lagrange, M. E I Makrini, and A. Hérold, *Carbon* **18**, 257 (1980).
- <sup>27</sup>T. S. Toellner, A. Alatas, A. Said, D. Shu, W. Sturhahn, and J. Zhao, *J. Synch. Radiat.* **13**, 211 (2006).
- <sup>28</sup>L. Boeri, G. B. Bachelet, M. Giantomassi, and O. K. Andersen, *Phys. Rev. B* **76**, 064510 (2007).
- <sup>29</sup>E. Burkel, *Rep. Prog. Phys.* **63**, 171 (2000).
- <sup>30</sup>The large IXS intensity at low-energy transfer in the CaC<sub>6</sub> "3D powder" simulations arises from the low-energy phonons predicted around the X point in the Brillouin zone [shown in Fig. 1(d)], which are intense because the IXS cross section is inversely proportional to energy transfer.
- <sup>31</sup>M. H. Upton, T. R. Forrest, A. C. Walters, C. A. Howard, M. Ellerby, A. H. Said, and D. F. McMorrow, *Phys. Rev. B* **82**, 134515 (2010).
- <sup>32</sup>S. Funahashi, T. Kondow, and M. Iizumi, *Physica B* **120**, 305 (1983).
- <sup>33</sup>A. Magerl, H. Zabel, and J. J. Rush, *Synth. Met.* **7**, 339 (1983).